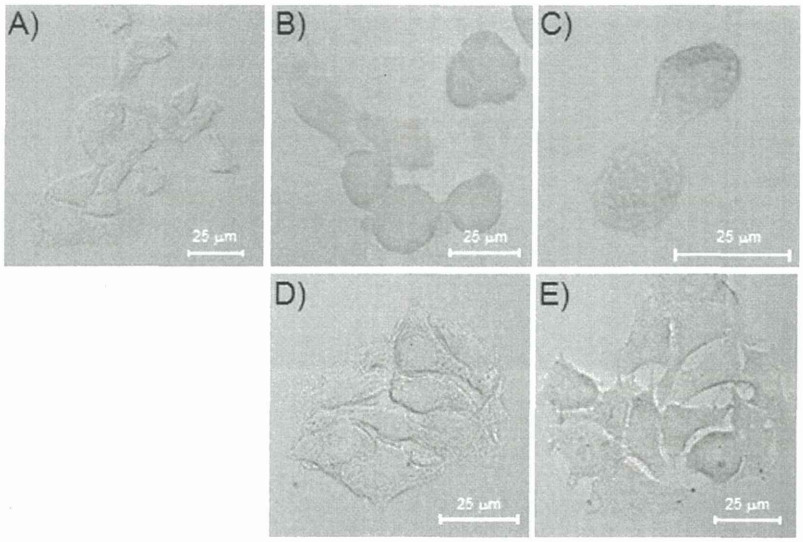

Figure 8. Microscopic images of HepG2 incubated for 24 h without SFNPs (A), with 5 μg/mL of CdTe/CdS βGal-SFNPs (B), with 50 μg/mL of CdTe/CdS βGal-SFNPs (C), with 5 μg/mL of ZAIS/ZnS βGal-SFNPs (D), and with 50 μg/mL of ZAIS/ZnS βGal-SFNPs (E).

1 and **2** slightly suppressed the cytotoxicity of CdTe/CdS QDs. In the morphological study, cells treated with CdTe/CdS SFNPs showed shrinkage, exhibiting cytotoxicity that may be caused by Cd^{2+} ions.[38] Thus, our newly developed ZAIS/ZnS SFNPs appear to be highly promising tools for in vitro and in vivo cell analysis because of their negligible cytotoxicity.

In this study, we successfully synthesized cadmium-free SFNPs containing low-toxicity ZAIS/ZnS NPs as the core and demonstrated their usefulness in the visual and fluorescent detection of sugar-chain–protein interactions, as well as in cellular imaging. The sugar-chain–ligand conjugate was easily immobilized onto the ZAIS NP surface by a simple ligand exchange reaction and could be applied to various sugar-chain–ligand conjugates. The binding interaction of the SFNPs with lectin was detected visually and spectroscopically. In flow cytometry analysis and cellular imaging, the binding properties of the SFNPs were diverse depending on the cell type, which may have great potential for profiling cells based on their sugar-chain binding properties. The results of the cytotoxicity assay showed that ZAIS/ZnS SFNPs were less toxic than CdTe/CdS SFNPs. Thus, our developed SFNPs are environmentally friendly compared with other cadmium-based semiconductor NPs and are likely to prove significantly useful for investigating various sugar-chain functions.

AUTHOR INFORMATION

Corresponding Authors

*TEL: (+81)99-285-7843, FAX: (+81)99-285-7856, E-mail: wakao@eng.kagoshima-u.ac.jp.
*TEL and FAX: (+81)99-285-8369.

Notes

The authors declare no competing financial interest.

ACKNOWLEDGMENTS

The present study was financially supported in part by grants from Japan Science and Technology Agency (Evolutionally venture program V07-05 to Y.S., CREST to Y.S., Research for Promoting Technological Seeds 16-057 to M.W., A-STEP AS242Z02646P to M.W.).

REFERENCES

(1) Varki, A. (1993) Biological roles of oligosaccharides: all of the theories are correct. *Glycobiology 3*, 97–130.
(2) Opdenakker, G., Rudd, P. M., Ponting, C. P., and Dwek, R. A. (1993) Concepts and princiles of Glycobiology. *FASEB J. 7*, 1330–1337.
(3) Park, S., and Shin, I. (2002) Fabrication of carbohydrate chips for studying protein-carbohydrate interactions. *Angew. Chem., Int. Ed. 41*, 3180–3182.
(4) Wang, D., Liu, S., Trummer, B. J., Deng, C., and Wang, A. (2002) Carbohydrate microarrys for the recognition of cross-reactive molecular markers of microbes and host cells. *Nat. Biotechnol. 20*, 275–281.
(5) Fukui, S., Feizi, T., Galustian, C., Lawson, A. M., and Chai, W. (2002) Oligosaccharide microarrays for high-throughput detection and specificity assignments of carbohydrate-protein interactions. *Nat. Biotechnol. 20*, 1011–1017.
(6) Fazio, F., Bryan, M. C., Blixt, O., Paulson, J. C., and Wong, C.-H. (2002) Synthesis of sugar arrays in microtiter plate. *J. Am. Chem. Soc. 124*, 14397–14402.
(7) Mann, D. A., Kanai, M., Maly, D. J., and Kiessling, L. L. (1998) Probing low affinity and multivalent interactions with surface plasmon resonance: ligands for concanavalin A. *J. Am. Chem. Soc. 120*, 10575–10582.
(8) Horan, N., Yan, L., Isobe, H., Whitesides, G. M., and Kahne, D. (1999) Nonstatical binding of a protein to clustered carbohydrates. *Proc. Natl. Acad. Sci. U.S.A. 96*, 11782–11786.
(9) Oyelaran, O., and Gildersleeve, J. C. (2009) Glycan arrays: recent advances and future challenges. *Curr. Opin. Chem. Biol. 13*, 406–413.
(10) Hase, S., Ibuki, T., and Ikenaka, T. (1984) Reexamination of the pyridylamination used for fluorescence labeling of oligosaccharides and its application to glycoproteins. *J. Biochem. 95*, 197–203.
(11) Anumula, K. R. (2006) Advances in fluorescence derivatization methods for high-performance liquid chromatographic analysis of glycoprotein carbohydrates. *Anal. Biochem. 350*, 1–23.
(12) Reddington, M. V. (1998) New glycoconjugated cyanine dyes as fluorescent labeling reagents. *J. Chem. Soc., Perkin Trans.*, 143–147.

(13) Gege, C., Oscarson, S., and Schmidt, R. R. (2001) Synthesis of fluorescence labeled sialyl lewis(x) glycosphingolipids. *Tetrahedron Lett. 42*, 377−380.
(14) de la Fuente, J. M., Barrientos, A. G., Rojas, T. C., Rojo, J., Cañada, J., Fernández, A., and Penadés, S. (2001) Gold glyconanoparticles as water-soluble polyvalent models to study carbohydrate interactions. *Angew. Chem., Int. Ed. 40*, 2258−2261.
(15) Osaki, F., Kanamori, T., Sando, S., Sere, T., and Aoyama, Y. (2004) A quantum dot conjugated sugar ball and its cellular uptake. on the size effects of endocytosis in the subviral region. *J. Am. Chem. Soc. 126*, 6520−6521.
(16) Sun, X.-L., Cui, W., Haller, C., and Chaikof, E. L. (2004) Site-specific multivalent carbohydrate labeling of quantum dots and magnetic beads. *ChemBioChem 5*, 1593−1596.
(17) de la Fuente, J. M., and Penadés, S. (2005) Glyco-quantum dots: a new luminescent system with multivalent carbohydrate display. *Tetrahedron: Asymmetry 16*, 387−391.
(18) Robinson, A., Fang, J.-M., Chou, P.-T., Liao, K.-W., Chu, R.-M., and Lee, S.-J. (2005) Probing lectin and sperm with carbohydrate-modified quantum dots. *ChemBioChem 6*, 1899−1905.
(19) Babu, P., Sinha, S., and Surolia, A. (2007) Sugar-quantum dot conjugates for selective and sensitive detection of lectins. *Bioconjugate Chem. 18*, 146−151.
(20) Niikura, K., Nishio, T., Akita, H., Matsuo, Y., Kamitani, R., Kogure, K., Harashima, H., and Ijiro, K. (2007) Accumulation of O-GlcNAc-displaying CdTe quantum Dots in cells in the presence of ATP. *ChemBioChem 8*, 379−384.
(21) Kikkeri, R., Lepenies, B., Adibekian, A., Laurino, P., and Seeberger, P. H. (2009) In vivo imaging and in vitro liver targeting with carbohydrate capped quantum dots. *J. Am. Chem. Soc. 131*, 2110−2112.
(22) Marradi, M., Martín-Lomas, M., and Penadés, S. (2010) Glyconanoparticles: polyvalent tools to study carbohydrate-based interactions. *Adv. Carbohydr. Chem. Biochem. 64*, 211−290.
(23) Varki, A., and Marth, J. (1995) Oligosaccharides in vertebrate development. *Semin. Dev. Biol. 6*, 127−138.
(24) Gabius, H.-J., André, S., Kaltner, H., and Siebert, H.-C. (2002) The sugar code: functional lectinomics. *Biochim. Biophys. Acta 1572*, 165−177.
(25) Sharon, N., and Lis, H. (2004) History of lectins: from hemagglutinins to biological recognition molecules. *Glycobiology 14*, 53R−62R.
(26) Ilyin, S. E., Belkowski, S. M., and Plata-Salamán, C. R. (2004) Biomarker discovery and validation: technologies and integrative approaches. *TRENDS Biotechnol. 22*, 411−416.
(27) Rifai, N., Gillette, M. A., and Carr, S. A. (2006) Protein biomarker discovery and validation: the long and uncertain path to clinical utility. *Nat. Biotechnol. 24*, 971−983.
(28) Nagano, K., Yoshida, Y., and Isobe, T. (2008) Cell surface biomarkers of embryonic stem cells. *Proteomics 8*, 4025−4035.
(29) Tateno, H., Uchiyama, N., Kuno, A., Togayachi, A., Sato, T., Narimatsu, H., and Hirabayashi, J. (2007) A novel strategy for mammalian cell surface glycome profiling using lectin microarray. *Glycobiology 17*, 1138−1146.
(30) Toyoda, M., Yamazaki-Inoue, M., Itakura, Y., Kuno, A., Ogawa, T., Yamada, M., Akutsu, H., Takahashi, Y., Kanzaki, S., Narimatsu, H., Hirabayashi, J., and Umezawa, A. (2011) Lectin microarray analysis of pluripotent and multipotent stem cells. *Genes Cells 16*, 1−11.
(31) Jeong, H. H., Kim, Y. G., Jang, S. C., Yi, H., and Lee, C. S. (2012) Profiling surface glycan on live cells and tissues using quantum dot-lectin nanoconjugates. *Lab Chip 12*, 3290−3295.
(32) Nishijima, Y., Toyoda, M., Yamazaki-Inoue, M., Sugiyama, T., Miyazawa, M., Muramatsu, T., Nakamura, K., Narimatsu, H., Umezawa, A., and Mikami, M. (2012) Glycan profiling of endometrial cancers using lectin microarray. *Genes Cells 17*, 826−836.
(33) Alivisatos, A. P. (1996) Semiconductor clusters, nanocrystals, and quantum dots. *Science 271*, 933−937.
(34) Bruchez, M., Moronne, M., Gin, P., Weiss, S., and Alivistos, A. P. (1998) Semiconductor nanocrystals as fluorescent biological labels. *Science 281*, 2031−2016.
(35) Chan, W. C. W., and Nie, S. M. (1998) Quantum dot bioconjugates for ultrasensitive nonisotopic detection. *Science 281*, 2016−2018.
(36) Akerman, M. E., Chan, W. C. W., Laakkonen, P., Bhatia, S. N., and Ruslahti, E. (2002) Nanocrystal targeting in vivo. *Proc. Natl. Acad. Sci. U.S.A. 99*, 12617−12621.
(37) Walling, M. A., Novak, J. A., and Shepard, J. R. E. (2009) Quantum dots for live cell and in vivo imaging. *Int. J. Mol. Sci. 10*, 441−491.
(38) Ipe, B. I., Lehnig, M., and Niemeyer, C. M. (2005) On the generation of free radical species from quantum dots. *Small 1*, 706−709.
(39) Hardman, R. (2006) A toxicologic review of quantum dots: toxicity depends on physicochemical and environmental factors. *Env. Health Persp. 114*, 116−172.
(40) Chang, E., Thekkek, N., Yu, W. W., Colvin, V. L., and Drezek, R. (2006) Evaluation of quantum dot cytotoxicity based on intracellular uptake. *Small 2*, 1412−1417.
(41) Chang, S.-Q., Dai, Y.-D., Kang, B., Han, W., Mao, L., and Chen, D. (2009) UV-enhanced cytotoxicity of thiol-capped CdTe quantum dots in human pancreatic carcinoma cells. *Toxicol. Lett. 188*, 104−111.
(42) Rzigalinski, B. A., and Strobl, J. S. (2009) Cadmium-containing nanoparticles: perspectives on pharmacology and toxicology of quantum dots. *Toxicol. Appl. Pharmacol. 238*, 280−288.
(43) Ballou, B., Lagerholm, B. C., Ernst, L. A., Bruchez, M. P., and Waggoner, A. S. (2004) Noninvasive imaging of quantum dots in mice. *Bioconjugate Chem. 15*, 79−86.
(44) Hoshino, A., Fujioka, K., Oku, T., Suga, M., Sasaki, F. Y., Ohta, T., Yasuhara, M., Suzuki, K., and Yamamoto, K. (2004) Physicochemical properties and cellular toxicity of nanocrystal quantum dots depend on their surface modification. *Nano Lett. 4*, 2163−2169.
(45) Shiohara, A., Hoshino, A., Hanaki, K., Suzuki, K., and Yamamoto, K. (2004) On the cytotoxicity of quantum dots. *Microbiol. Immunol. 48*, 669−675.
(46) Kim, J., Park, Y., Yoon, T. H., Yoon, C. S., and Choi, K. (2010) Phototoxicity of CdSe/ZnSe quantum dots with surface coatings of 3-mercaptopropionic acid or tri-*n*-octylphosphine oxide/gum arabic in Daphnia magna under environmentally relevant UV-B light. *Aquatic Toxicol. 97*, 116−124.
(47) Suda, Y., Arano, A., Fukui, Y., Koshida, S., Wakao, M., Nishimura, T., Kusumoto, S., and Sobel, M. (2006) Immobilization and clustering of structurally defined oligosaccharides for sugar chips:an improved method for surface plasmon resonance analysis of protein−carbohydrate interactions. *Bioconjugate Chem. 17*, 1125−1135.
(48) Zhang, X., Nakamura-Tsuruta, S., Haruyama, M., Yokoyama, R., Nagatomo, M., Wakao, M., Nakajima, K., Aoyama, K., Okuno, T., Morikawa, S., Hiroi, S., Kase, T., Nose, H., Nishi, J., Okamoto, M., Baba, M., and Suda, Y. (2012) Super sensitive detection of viruses using sugar-chain immobilized gold nano-particles (SGNPs). *Polym. Prepr. 53*, 671−672.
(49) Shinchi, H., Wakao, M., Nakagawa, S., Mochizuki, E., Kuwabata, S., and Suda, Y. (2012) Stable sugar-chain immobilized fluorescent nano-particle for probing lectin and cells. *Chem.-Asian J. 7*, 2678−2682.
(50) Torimoto, T., Adachi, T., Okazaki, K., Sakuraoka, M., Shibayama, T., Ohtani, B., Kudo, A., and Kuwabata, S. (2007) Facile synthesis of ZnS-$AgInS_2$ solid solution nanoparticles for color-adjustable luminophore. *J. Am. Chem. Soc. 129*, 12388−12389.
(51) Torimoto, T., Ogawa, S., Adachi, T., Kameyama, T., Okazaki, K., Shibayama, T., Kudo, A., and Kuwabata, S. (2010) Remarkable photoluminescence enhancement of ZnS-$AgInS_2$ solid solution nanoparticles by postsynthesis treatment. *Chem. Commun. 46*, 2082−2084.

(52) Mosmann, T. (1983) Rapid colorimetric assay for cellular growth and survival: application to proliferation and cytotoxicity assays. *J. Immun. Methods. 65*, 55–63.
(53) Kuzuya, T., Tai, Y., Yamamuro, S., and Sumiyama, K. (2005) Synthesis of copper and zinc sulfide nanocrystals via thermolysis of the polymetallic thiolate cage. *Sci. Technol. Adv. Mater. 6*, 84–90.
(54) Castro, S. L., Bailey, S. G., Raffaelle, R. P., Banger, K. K., and Hepp, A. F. (2003) Nanocrystalline chalcopyrite materials ($CuInS_2$ and $CuInSe_2$) via low-temperature pyrolysis of molecurlar single-source precursors. *Chem. Mater. 15*, 3142–3147.
(55) Li, L., Daou, T. J., Texier, I., and Kim, T. T. (2009) Highly luminescent $CuInS_2$/ZnS core/shell nanocrystals: cadmium-free quantum dots for in vivo imaging. *Chem. Mater. 21*, 2422–2429.
(56) Pons, T., Pic, E., Lequeux, N., Cassette, E., Bezdetnaya, L., Guillemin, F., Marchal, F., and Dubertret, B. (2010) Cadmium-free $CuInS_2$/ZnS quantum dots for sentinel lymph node imaging with reduced toxicity. *ACS Nano 4*, 2531–2538.
(57) Matsumoto, T., Maenosono, S., and Yamaguchi, Y. (2004) Organometallic synthesis of InP quantum dots using tris-(dimethylamino)phosphine as a phosphorus source. *Chem. Lett. 33*, 1492–1493.
(58) Li, C., Ando, M., Enomoto, H., and Murase, N. (2008) Highly luminescent water-soluble InP/ZnS nanocrystals prepared via reactive phase transfer and photochemical processing. *J. Phys. Chem. C 112*, 20190–20199.
(59) Roe, J. H. (1955) The determination of sugar in blood and spinal fluid with anthrone reagent. *J. Biol. Chem. 212*, 335–343.
(60) Prasuhn, E. D., Deschamps, J. R, Susumu, K., Stewart, M. H., Boeneman, K., Blanco-Canosa, J. B., Dawson, P. E., and Medintz, I. L. (2010) Polyvalent display and packing of peptides and proteins on semiconductor quantum dots: predicted versus experimental results. *Small 6*, 555–564.
(61) Nakamura-Tsuruta, S., Kishimoto, Y., Nishimura, T., and Suda, Y. (2008) One-step purification of lectins from Banana pulp using sugar-immobilized gold nano-particles. *J. Biochem. 143*, 833–839.
(62) Wood, I. S., and Trayhurn, P. (2003) Glucose transporters (GLUT and SGLT): expanded families of sugar transport proteins. *Br. J. Nutr. 89*, 3–9.
(63) Stahl, P. D. (1992) The mannose receptor and other macrophage lectins. *Curr. Opin. Immunol. 4*, 49–52.
(64) Sato, S., and Hughes, R. C. (1994) Regulation of secretion and surface expression of Mac-2, a galactoside-binding protein of macrophages. *J. Biol. Chem. 269*, 4424–4430.
(65) Sano, H., Hsu, D. K., Apgar, J. R., Yu, L., Sharma, B. B., Kuwabara, I., Izui, S., and Liu, F.-T. (2003) Critical role of galectin-3 phagocytosis by macrophages. *J. Clin. Invest. 112*, 389–397.
(66) Crocker, P. R., Mucklow, S., Bouckson, V., McWilliam, A., Willis, A. C., Gordon, S., Milon, G., Kelm, S., and Bradfield, P. (1994) Sialoadhesin, a macrophage sialic acid binding receptor for haemopoietic cells with 17 immunoglobulin-like domains. *EMBO J. 13*, 4490–4503.
(67) Jones, C., Virji, M., and Crocker, R. (2003) Recognition of sialylated meningococcal lipopolysaccharide by siglecs expressed on myeloid cells leads to enhanced bacterial uptake. *Mol. Microbiol. 49*, 1213–1225.
(68) Baenziger, J. U., and Fiete, D. (1980) Galactose and N-acetylgalactosamaine-specific endocytosis of glycopeptides by isolated rat hepatocytes. *Cell 22*, 611–620.
(69) Ashwell, G., and Harford, J. (1982) Carbohydrate-specific receptors of the liver. *Annu. Rev. Biochem. 51*, 531–554.
(70) Braun, J. R., Willnow, T. E., Ishibashi, S., Ashwell, G., and Herz, J. (1996) Sugar chains, lipids, and other natural products. *J. Biol. Chem. 271*, 21160–21166.
(71) Raju, T. S., Briggs, J. B., Chamow, S. M., Winkler, M. E., and Jones, A. J. S. (2001) Glycoengineering of therapeutic glycoproteins: in vitro galactosylation and sialylation of glycoproteins with terminal N-acetylglucosamine and galactose residue. *Biochemistry 40*, 8868–8876.

EWS/ATF1 expression induces sarcomas from neural crest–derived cells in mice

Kazunari Yamada,[1,2] Takatoshi Ohno,[1] Hitomi Aoki,[3] Katsunori Semi,[4,5] Akira Watanabe,[4,5] Hiroshi Moritake,[6] Shunichi Shiozawa,[7] Takahiro Kunisada,[3] Yukiko Kobayashi,[8] Junya Toguchida,[4,8,9] Katsuji Shimizu,[1] Akira Hara,[2] and Yasuhiro Yamada[2,4,5]

[1]Department of Orthopedic Surgery, [2]Department of Tumor Pathology, and [3]Department of Tissue and Organ Development Regeneration and Advanced Medical Science, Gifu University Graduate School of Medicine, Gifu, Japan.
[4]Center for iPS Cell Research and Application (CiRA) and [5]Institute for Integrated Cell-Material Sciences, (WPI-iCeMS), Kyoto University, Kyoto, Japan.
[6]Division of Pediatrics, Department of Reproductive and Developmental Medicine, Faculty of Medicine, University of Miyazaki, Miyazaki, Japan.
[7]Department of Medicine, Kyushu University Beppu Hospital, Beppu, Japan. [8]Department of Tissue Regeneration, Institute for Frontier Medical Sciences, and [9]Department of Orthopaedic Surgery, Kyoto University, Kyoto, Japan.

Clear cell sarcoma (CCS) is an aggressive soft tissue malignant tumor characterized by a unique t(12;22) translocation that leads to the expression of a chimeric *EWS/ATF1* fusion gene. However, little is known about the mechanisms underlying the involvement of *EWS/ATF1* in CCS development. In addition, the cellular origins of CCS have not been determined. Here, we generated *EWS/ATF1*-inducible mice and examined the effects of *EWS/ATF1* expression in adult somatic cells. We found that forced expression of *EWS/ATF1* resulted in the development of *EWS/ATF1*-dependent sarcomas in mice. The histology of *EWS/ATF1*-induced sarcomas resembled that of CCS, and *EWS/ATF1*-induced tumor cells expressed CCS markers, including S100, SOX10, and MITF. Lineage-tracing experiments indicated that neural crest–derived cells were subject to *EWS/ATF1*-driven transformation. EWS/ATF1 directly induced Fos in an ERK-independent manner. Treatment of human and *EWS/ATF1*-induced CCS tumor cells with FOS-targeted siRNA attenuated proliferation. These findings demonstrated that FOS mediates the growth of *EWS/ATF1*-associated sarcomas and suggest that FOS is a potential therapeutic target in human CCS.

Introduction

Clear cell sarcoma (CCS) is an aggressive malignancy of adolescents and young adults that was first described by Enzinger (1). It typically arises in the deep soft tissues of the lower extremities closed to tendon, fascia, and aponeurosis (2). Chemotherapy and radiotherapy are not of any benefit (3–5), and a high rate of local and distant recurrence results in poor survival rates (3, 6, 7). CCSs harbor the potential for melanocytic differentiation and melanin synthesis (8). Gene expression profiles support the classification of CCS as a distinct genomic subtype of melanomas (9). These melanocytic features often make the distinction from malignant melanoma (MM) difficult. However, in contrast to MM, CCS is characterized by a chromosomal translocation, t(12;22)(q13;q12), that leads to the fusion of activating transcription factor 1 (*ATF1*) gene localized to 12q13 to Ewing's sarcoma oncogene (*EWS*) gene at 22q12 in up to 90% of cases, resulting in expression of the *EWS/ATF1* fusion gene (10–12). Given that CCS and MM have such similar characteristics, it has been proposed that CCSs may arise from a neural crest progenitor. However, the exact origin of CCS still remains to be determined.

The biological role of the EWS/ATF1 fusion protein is still unclear. EWS contains a transcriptional activation domain in the N-terminal region (13–15) and several conserved RNA binding motifs in the C-terminal region (16). Binding of the N-terminal region of EWS to the RNA polymerase II subunit hsRPB7 has been proposed to be important for transactivation of the target genes (17). In contrast, ATF1 is a member of the CREB transcription factor family, whose activity is regulated through phosphorylation of its kinase inducible domain (KID) by protein kinase A (18). ATF1 mediates the activation of cAMP-responsive genes through binding to a conserved cAMP-responsive element (CRE) as a dimmer (19, 20). However, the N-terminal activation domain of EWS replaces the KID in the EWS/ATF1 fusion protein, rendering it unable to support a typical inductive signal (21). Therefore, EWS/ATF1 can act as constitutive transcriptional activator in a cAMP-independent fashion with normal CRE DNA binding activity (14, 22, 23).

Previous studies have revealed some target genes of EWS/ATF1, but their true function in tumorigenesis is still not well understood (24). Expression of *MITF* is constitutively activated by *EWS/ATF1* in CCS in vitro (25). Consistent with this finding, several studies have identified the expression of MITF protein or mRNA in CCS (26–28). MITF is a master regulator of melanocyte development and plays a role in melanoma development (29, 30). Importantly, activation of MITF by EWS/ATF1 is required for CCS proliferation as well as for melanocytic differentiation of CCS in vitro (25).

Although previous studies have demonstrated that EWS/ATF1 is associated with oncogenic potential in CCS, the effect of in vivo expression of *EWS/ATF1* on sarcoma formation is still not known. In the present study, we established *EWS/ATF1* transgenic mice using a doxycycline-dependent expression system in order to investigate the role of *EWS/ATF1* on CCS development in vivo. Our results showed that forced expression of *EWS/ATF1* induced CCS-like sarcoma in the transgenic mice. This mouse model was used to identify the origin of *EWS/ATF1*-induced sarcomas as well as the direct target of EWS/ATF1 in these sarcomas.

Results

Inducible expression of EWS/ATF1 in mice. We first generated doxycycline-inducible *EWS/ATF1* ES cells, in which the human *EWS/ATF1* type 2 fusion gene (26, 31) can be induced under the control of

Conflict of interest: The authors have declared that no conflict of interest exists.
Citation for this article: *J Clin Invest.* doi:10.1172/JCI63572.

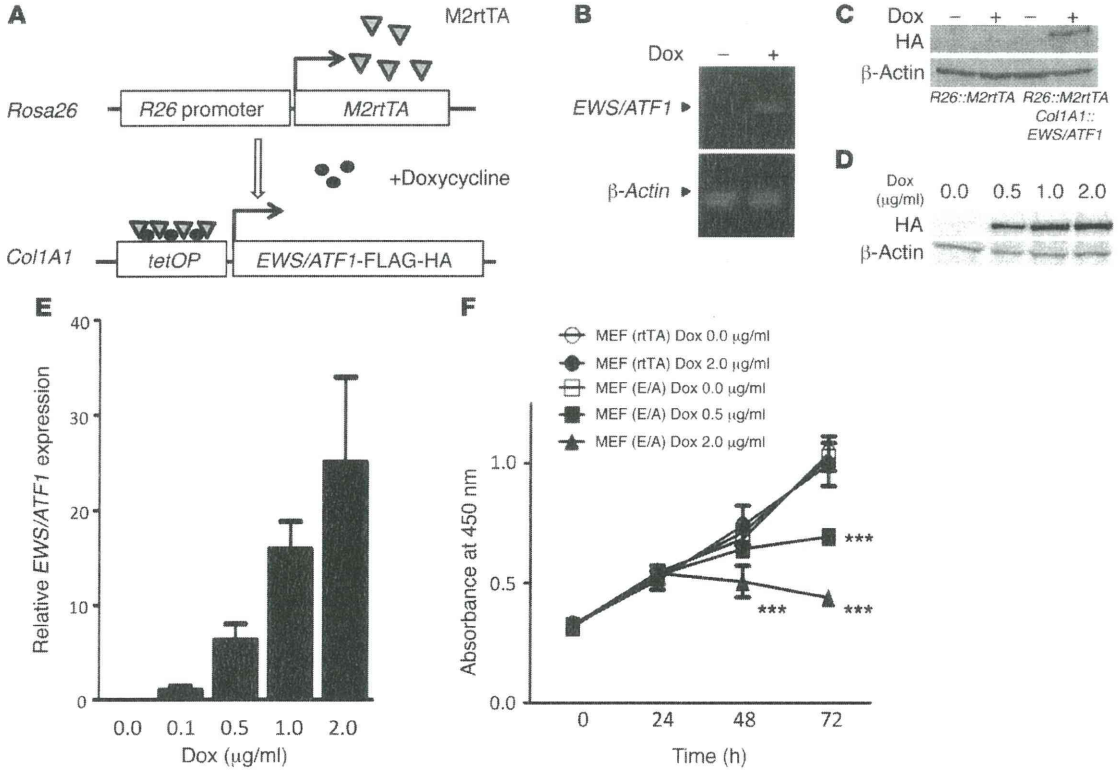

Figure 1

Inducible expression of *EWS/ATF1*. (**A**) Schematic of the doxycycline-inducible *EWS/ATF1* alleles. (**B**) *EWS/ATF1* expression in ES cells, detected by RT-PCR, after exposure to doxycycline for 12 hours. (**C**) EWS/ATF1 expression in ES cells, detected by Western blot, after exposure to doxycycline for 24 hours. (**D**) Dose-dependent induction of EWS/ATF1 protein in *EWS/ATF1*-inducible ES cells by doxycycline. ES cells were exposed to doxycycline concentrations up to 2 μg/ml for 24 hours. Western blot analysis was performed using an anti-HA antibody. (**E**) Dose-dependent doxycycline induction of *EWS/ATF1* mRNA in *EWS/ATF1*-inducible MEFs. MEFs were exposed to different concentrations of doxycycline for 24 hours. Transcript levels were normalized to β-*actin*. Data are mean ± SD ($n = 3$). (**F**) *EWS/ATF1* expression suppressed MEF growth. Cell viability was determined by WST-8 assay. Data are mean ± SD ($n = 4$). Control MEFs (rtTA) and *EWS/ATF1*-inducible MEFs (E/A) were derived from heterozygous *Rosa26::M2rtTA* and *Col1A1::tetO-EWS/ATF1* mice, respectively. ***$P < 0.001$ vs. MEF (rtTA) Dox 0.0 μg/ml, MEF (rtTA) Dox 2.0 μg/ml, and MEF (E/A) Dox 0.0 μg/ml.

a tetracycline-responsive regulatory element (Figure 1A). Upon treatment of these ES cells with doxycycline, expression of the *EWS/ATF1* fusion transcript was detected by RT-PCR (Figure 1B). We also confirmed the expression of EWS/ATF1 protein upon doxycycline treatment (Figure 1C), which was regulated in a dose-dependent manner (up to 2 μg/ml; Figure 1D).

Heterozygous *Rosa26::M2rtTA* mice with heterozygous *tetO-EWS/ATF1* allele were used to induce the *EWS/ATF1* fusion gene. Cultured murine embryonic fibroblasts (MEFs) derived from *EWS/ATF1*-inducible mice were first exposed to doxycycline to test the effect of *EWS/ATF1* expression on somatic cells. *EWS/ATF1* expression at the mRNA level was confirmed 24 hours after exposure (Figure 1E). Unexpectedly, the cell proliferation rate of MEFs decreased after *EWS/ATF1* induction in a doxycycline dose-dependent manner (Figure 1F).

EWS/ATF1 induces sarcoma formation in mice. To investigate the effect of *EWS/ATF1* expression in vivo, we treated *EWS/ATF1*-inducible mice at 6 weeks of age with doxycycline in the drinking water (50 μg/ml). The *EWS/ATF1*-inducible mice given doxycycline started to develop multiple macroscopic soft tissue tumors after 4 weeks. After doxycycline treatment, EWS/ATF1 protein was detected in a variety of tissues, including the intestine, liver, epidermis, and deep soft tissue (Supplemental Figure 1A; supplemental material available online with this article; doi:10.1172/JCI63572DS1). Doxycycline treatment for 3 months resulted in tumor formation in the deep soft tissues of all mice ($n = 39$), whereas control mice without doxycycline treatment developed no detectable tumors. *EWS/ATF1*-induced tumors typically arose in the trunks, heads, limbs, and whisker pads (Figure 2A). Macroscopically, tumors consisted of circumscribed and lobulated gray-white mass (Figure 2A). In most cases, the tumors were attached to fascia or aponeuroses (Figure 2, A and B), which indicates that the tumors specifically arose from the deep soft tissues. Importantly, 36 of 39 mice (92%) developed tumors in the trunk, which suggests that cells located in the trunk are particularly permissive for tumorigenesis by *EWS/ATF1* expression. Despite expression of EWS/ATF1 protein, no tumor formation was observed in other tissues, such as the epidermis and intestine, even in mice given doxycycline for 3 months.

Microscopic examination of these tumors revealed striking similarities to human CCSs. The tumors showed a rather uniform pattern of compact nests or fascicles of rounded or fusiform cells, which were divided by a framework of fibrocollagenous tissue (Figure 2B).

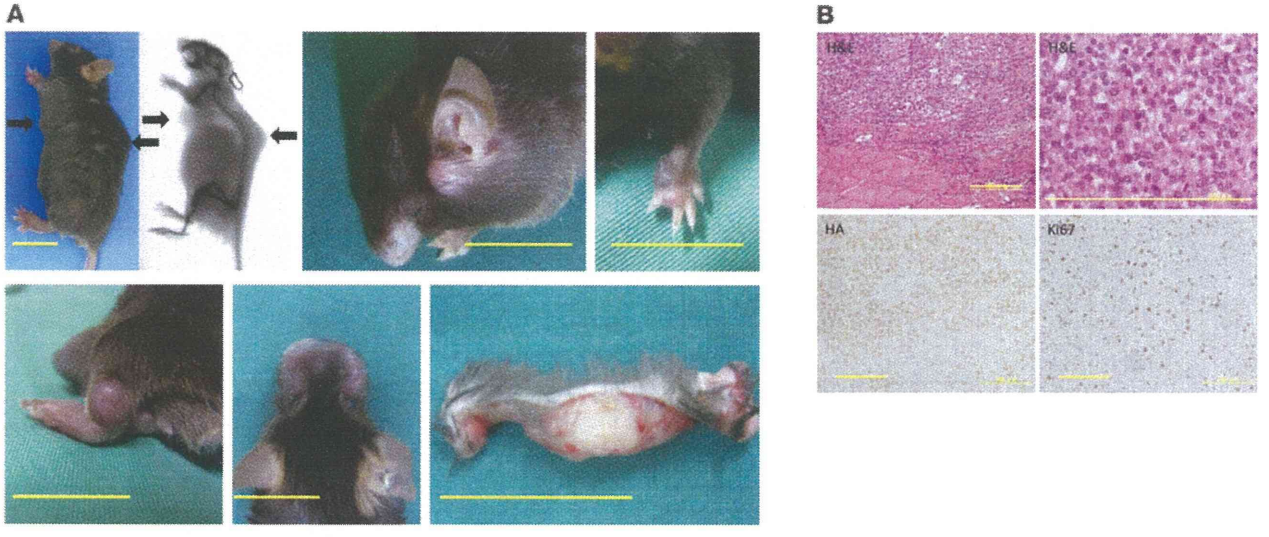

Figure 2

EWS/ATF1-induced tumors resemble human CCS. *EWS/ATF1* transgenic mice were administered 50 μg/ml doxycycline in their drinking water for 3 months. (**A**) *EWS/ATF1* expression caused tumor formation (arrows) in various locations: trunk, head, limbs, and whisker pads. X-ray examination revealed multiple tumors in deep soft tissue. The cut surface of a large tumor on the ventral trunk of an *EWS/ATF1*-inducible mouse revealed a lobulated gray-white mass in the deep soft tissue. Scale bars: 20 mm. (**B**) Histological analysis of *EWS/ATF1*-induced tumors. Tumors were composed of round or fusiform cells with prominent basophilic nuclei and clear cytoplasm, which were surrounded by fibrous fascicles. HA immunostaining confirmed EWS/ATF1 expression in the tumor cells. Frequent Ki67-positive cells were present throughout the lesions. Scale bars: 200 μm (H&E, left); 50 μm (H&E, right); 100 μm (HA and Ki67).

The individual tumor cells had a homogeneous appearance. They had round to ovoid vesicular nuclei with prominent basophilic nucleoli and clear or pale-staining cytoplasm (Figure 2B). The majority of the tumor cells expressed EWS/ATF1 fusion protein in nuclei (Figure 2B and Supplemental Figure 2A). Ki67-positive proliferating cells were observed in about 30%–40% of tumor cells (Figure 2B), indicative of active proliferative activity. The survival curves of *EWS/ATF1*-induced mice were analyzed to evaluate the overall effect of *EWS/ATF1* expression on life span. The transgenic mice treated with doxycycline became moribund within 3–10 months, suggestive of multiple tumor formation in the deep soft tissue, whereas mice without doxycycline treatment survived much longer, and no tumor formation was observed. The median survival time of *EWS/ATF1*-inducible mice treated with doxycycline was 20 weeks (Supplemental Figure 2B).

Previous studies demonstrated that human CCSs express markers for neural crest lineage as well as melanocytic differentiation (8, 9). Therefore, to examine the similarity of mouse *EWS/ATF1*-induced tumors with human CCSs, we performed immunohistochemical analysis for CCS-expressing markers; *EWS/ATF1*-induced tumor cells showed the expression such markers, including S100, Sox10, and Mitf (Figure 3A).

Neural crest–lineage cells are permissive to EWS/ATF1-driven sarcoma development. The cell of origin for CCS remains to be determined. Based on the potential of CCSs for melanocytic differentiation and melanin synthesis, previous studies proposed that CCS may arise from a neural crest progenitor. To determine whether *EWS/ATF1*-induced sarcomas actually arise from neural crest–derived cells, we performed a lineage-tracing experiment in which neural crest–derived cells were tagged by reporter in vivo (32). To label neural crest–derived cells in vivo, we first used transgenic mice containing *Wnt1-Cre* and floxed *LacZ* reporter alleles. We further introduced doxycycline-inducible *EWS/ATF1* alleles into the reporter mice to generate compound transgenic mice (Figure 3B). We confirmed that *EWS/ATF1*-induced tumor cells did not express *Wnt1* (Supplemental Figure 3A). Transgenic mice were treated with doxycycline in the drinking water to induce subcutaneous tumors and the developed tumors were then analyzed for the expression of the reporter gene. Importantly, all 14 *EWS/ATF1*-induced tumors were ubiquitously positive for X-gal staining (Figure 3C and Supplemental Figure 3D), which suggests that neural crest–lineage cells are a cell of origin for *EWS/ATF1*-associated sarcomas. We further performed another lineage-tracing experiment using transgenic mice containing *P0-Cre* and floxed *EYFP* reporter alleles (Figure 3D), which have been also widely used to label neural crest–derived cells. Again, we found that all 6 *EWS/ATF1*-induced tumors were positive for EYFP (Figure 3E and Supplemental Figure 4, C and D).

Establishment of tumor cell lines. Tumor samples were obtained from primary tumors of *EWS/ATF1*-induced mice to establish cell lines from *EWS/ATF1*-induced tumors. We established 2 tumor cell lines, G1297 and G1169, from 2 independent mice. These cells grew in the form of an adherent monolayer in the presence of doxycycline (0.2 μg/ml). We cultured the cells up to the fourth passage in medium containing 0.2 μg/ml doxycycline in order to avoid contamination by fibroblasts. We examined the effect of different concentrations of doxycycline on the growth and morphology of the established cell lines. We confirmed that the expression of *EWS/ATF1* transcript and protein increased in response to doxycycline in a dose-dependent manner in both established cell lines (Supplemental Figure 5, A–C). The growth and morphology of the tumor cells varied in a doxycycline dose-dependent manner: small, round tumor cells grew rapidly at concentrations above 0.1 μg/ml,

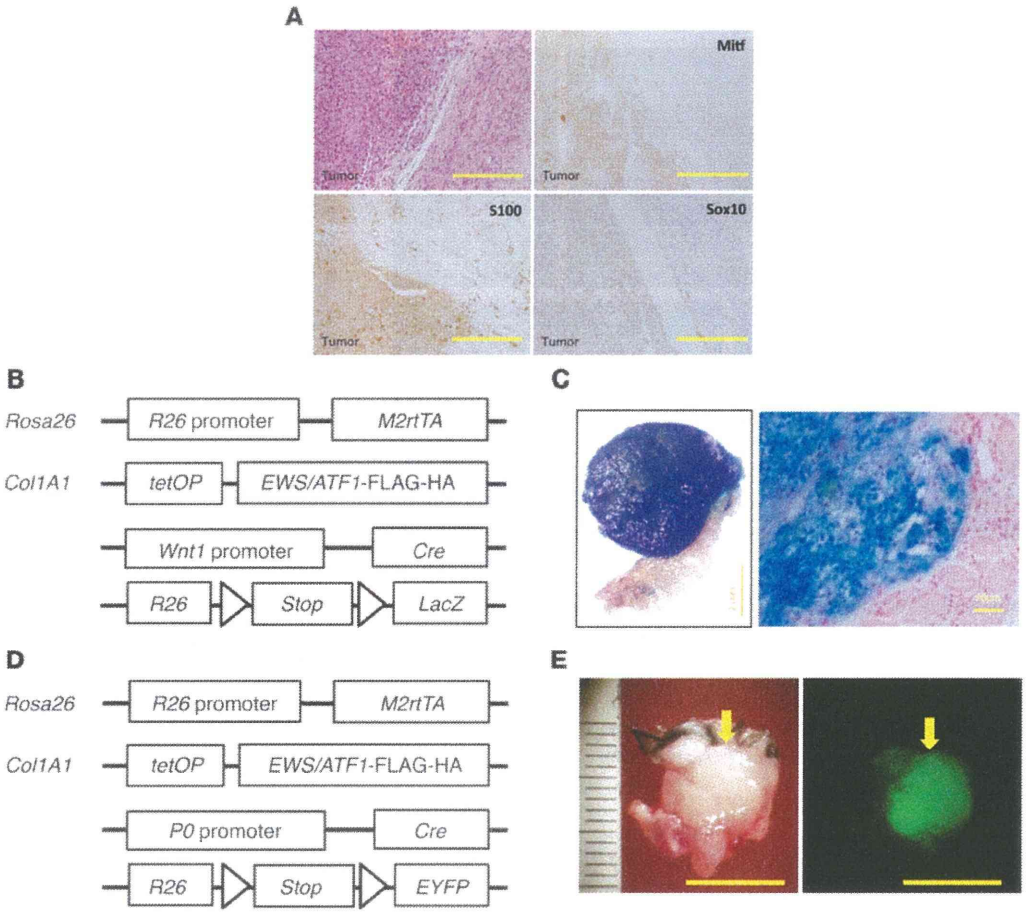

Figure 3

EWS/ATF1-induced tumors arise from neural crest–lineage cells. (**A**) Immunohistochemical analysis for CCS markers. Nuclear staining for S100, Sox10, and Mitf was observed in tumor cells. Sections were counterstained with hematoxylin. Scale bars: 100 μm. (**B**) Schematic representation of reporter alleles for the lineage-tracing experiment using *Wnt1-Cre* allele. Doxycycline-inducible *EWS/ATF1* alleles were introduced into reporter mice containing the *Wnt1-Cre* and floxed *LacZ* reporter alleles. (**C**) X-gal staining for *EWS/ATF1*-induced tumors with *Wnt1-Cre* and floxed *LacZ* reporter alleles. Positive staining for X-gal indicated that the tumor arose from a neural crest–lineage cell. Histological analysis revealed that neoplastic cells were stained with X-gal. Counterstaining was performed with fast red. Scale bars: 2 mm (left); 50 μm (right). (**D**) Schematic representation of reporter alleles for the lineage-tracing experiment using *P0-Cre* allele. Doxycycline-inducible *EWS/ATF1* alleles were introduced into reporter mice containing the *P0-Cre* and floxed *EYFP* reporter alleles. (**E**) Representative image of a tumor (arrow) in the trunk of an *EWS/ATF1*-induced mouse with *P0-Cre* and floxed *EYFP* reporter alleles. Fluorescent signals for EYFP expression were detected in the. Scale bars: 10 mm.

whereas dendritic fibroblast–like spindle cells were observed below 0.05 μg/ml (Figure 4A). Notably, doxycycline withdrawal caused rapid morphological changes, into a fibroblast-like shape, and these tumor cells did not proliferate up to the next passage (Figure 4A). Consistent with these findings, cell viability assay revealed that the number of cells was increased by doxycycline treatment in a dose-dependent manner (Figure 4B). We next examined the effect of *EWS/ATF1* expression on tumorigenesis ability in the subcutaneous tissue of immunocompromised mice. The established cell line G1297 was cultured in medium containing 0.2 μg/ml doxycycline, and 5.0×10^6 cells were transplanted into the subcutaneous tissue of nude mice. It is important to note that all mice treated with 50 μg/ml doxycycline in the drinking water developed tumors within 3 weeks, whereas no tumor formation was observed in mice without doxycycline treatment (Figure 4C). Histological analysis revealed that the subcutaneous tumors in nude mice consisted of neoplastic cells that resembled the primary tumor cells in *EWS/ATF1*-induced transgenic mice (Figure 4D). Positive immunoreactivity for HA-Tag was observed in all tumor cells (Figure 4D).

Continuous expression of EWS/ATF1 is required for tumor growth maintenance. To further examine whether continuous expression of *EWS/ATF1* is necessary for the growth of *EWS/ATF1*-induced tumors, we withdrew doxycycline in tumor-bearing EWS/ATF1 transgenic mice that had been given doxycycline for 3 months. Importantly, doxycycline withdrawal resulted in a rapid reduction of tumor mass in 4 independent mice (7 tumors total). The regressed tumors contained fibrous tissue, but no viable neoplastic cells were observed 3 months after doxycycline withdrawal (Figure 4E), which suggests that *EWS/ATF1*-induced tumor growth depends on continuous *EWS/ATF1* expression. We next examined the histological changes shortly after doxycycline withdrawal in order to investigate the mechanisms of tumor regression.

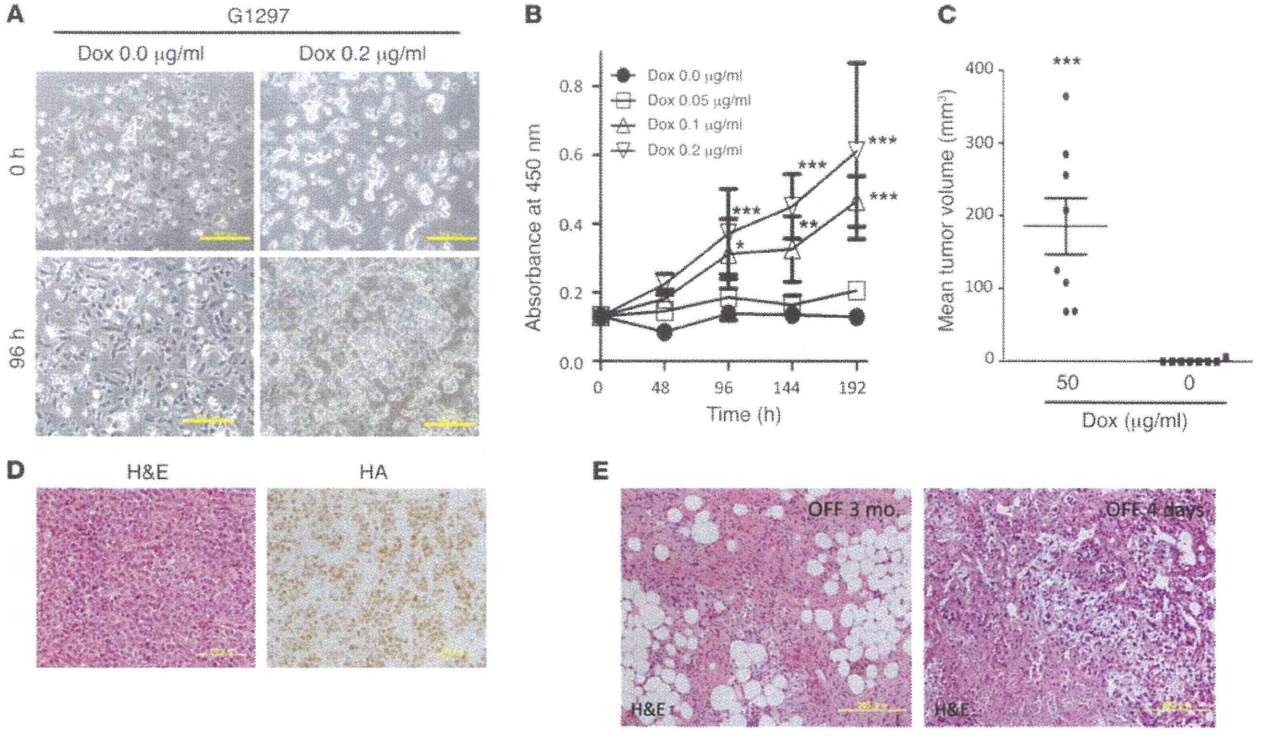

Figure 4

Establishment and analysis of tumor cell lines. G1297 and G1169 cell lines were established from 2 independent *EWS/ATF1*-induced tumors. (**A**) Morphology of the G1297 line after treatment without or with doxycycline (0 and 0.2 μg/ml, respectively). At concentrations above 0.1 μg/ml, small, round tumor cells grew rapidly, while dendritic fibroblast-like spindle cells were observed; tumor cell growth almost stopped at concentrations less than 0.05 μg/ml. Scale bars: 50 μm. (**B**) Effect of different levels of *EWS/ATF1* on tumor cell growth. G1297 cells were cultured in different concentrations of doxycycline (0, 0.05, 0.1, and 0.2 μg/ml), and cell viability was determined by WST-8 assay. Data are mean ± SD ($n = 8$). $^*P < 0.05$, $^{**}P < 0.01$, $^{***}P < 0.001$ vs. Dox 0.0 μg/ml. (**C**) Subcutaneous transplantation of 5.0×10^6 G1297 cells in immunocompromised mice resulted in tumor formation in mice treated with 50 μg/ml doxycycline ($n = 8$). Mean tumor volumes ± SEM are shown. $^{***}P < 0.005$. (**D**) Representative histology and HA immunostaining of tumors in nude mice. The tumor resembled the original sarcoma with EWS/ATF1 expression. Scale bars: 100 μm. (**E**) Doxycycline withdrawal led to rapid tumor regression. At 3 months after doxycycline withdrawal, no viable tumor cells were observed, and tumors were replaced by fibrous tissue. Widespread cell death was observed 4 days after doxycycline withdrawal. Scale bars: 200 μm.

We found widespread cell death within the tumor mass, accompanied by massive infiltration of inflammatory cells, at 4 days after doxycycline withdrawal (Figure 4E), which indicates that neoplastic cells cannot survive in vivo without *EWS/ATF1* expression. Taken together, these results clearly indicate that *EWS/ATF1* plays a pivotal role in the proliferation and maintenance of *EWS/ATF1*-induced tumor cells in vivo.

Fos is a direct target of EWS/ATF1. To determine the downstream targets regulated by EWS/ATF1, we next performed gene expression analysis using G1297 cells. First, we confirmed that withdrawal of doxycycline for 96 hours resulted in no detectable expression of *EWS/ATF1* RNA or protein in cultured tumor cells. Next, the tumor cells were exposed again to doxycycline at a concentration of 0.05 or 0.2 μg/ml, and microarray analysis was performed at 3 and 48 hours after doxycycline exposure. Induction of *EWS/ATF1* resulted in altered expression of a number of genes associated with cell growth, such as growth factor genes (*Areg* and *Ereg*), cell cycle regulators (*Cenpa*, *Ccna2*, *Ccnb2*, *Cdkn1b*, *Plk1*, and *Aurka*), and a proto-oncogene (*Fos*) at either time point (Supplemental Figure 6A). Although a previous study demonstrated that *MITF-M* is a direct target of EWS/ATF1 in human CCS cell lines (25), we failed to detect its expression in our *EWS/ATF1*-induced tumor cell lines and primary tumor samples (Supplemental Figure 7, A and B). Among the transcripts upregulated by *EWS/ATF1*, we focused on the proto-oncogene *Fos*, because this was one of the most highly upregulated genes by *EWS/ATF1* after doxycycline exposure in the microarray analysis (Supplemental Figure 6A). Quantitative real-time RT-PCR (qRT-PCR) confirmed upregulation of both *Fos* and *EWS/ATF1* transgenes in 2 independent tumor cell lines as early as 3 hours after doxycycline exposure (Figure 5A and Supplemental Figure 7C). We also found that the *EWS/ATF1*-induced tumor specimens expressed higher levels of both *Fos* and *EWS/ATF1* transgenes (Figure 5B). Expression of *Fos* is induced by numerous stimuli, which are transmitted through the RAS/Raf/MAP kinase or cAMP-dependent protein kinase pathway (33). In order to investigate the mechanism of *Fos* induction by *EWS/ATF1*, we next examined whether the RAS/Raf/MAP kinase pathway is involved in *EWS/ATF1*-mediated *Fos* activation. In contrast to the rapid and transient induction of Fos in MEFs after serum stimulation (Supplemental Figure 7D), expression of Fos in the *EWS/ATF1*-expressing tumor cell line was detected even under serum-free conditions, and it gradually increased after serum stimulation (Supplemental Figure 7E). Interestingly, whereas serum-stimulated MEFs revealed immediate phosphorylation of ERK1 and ERK2

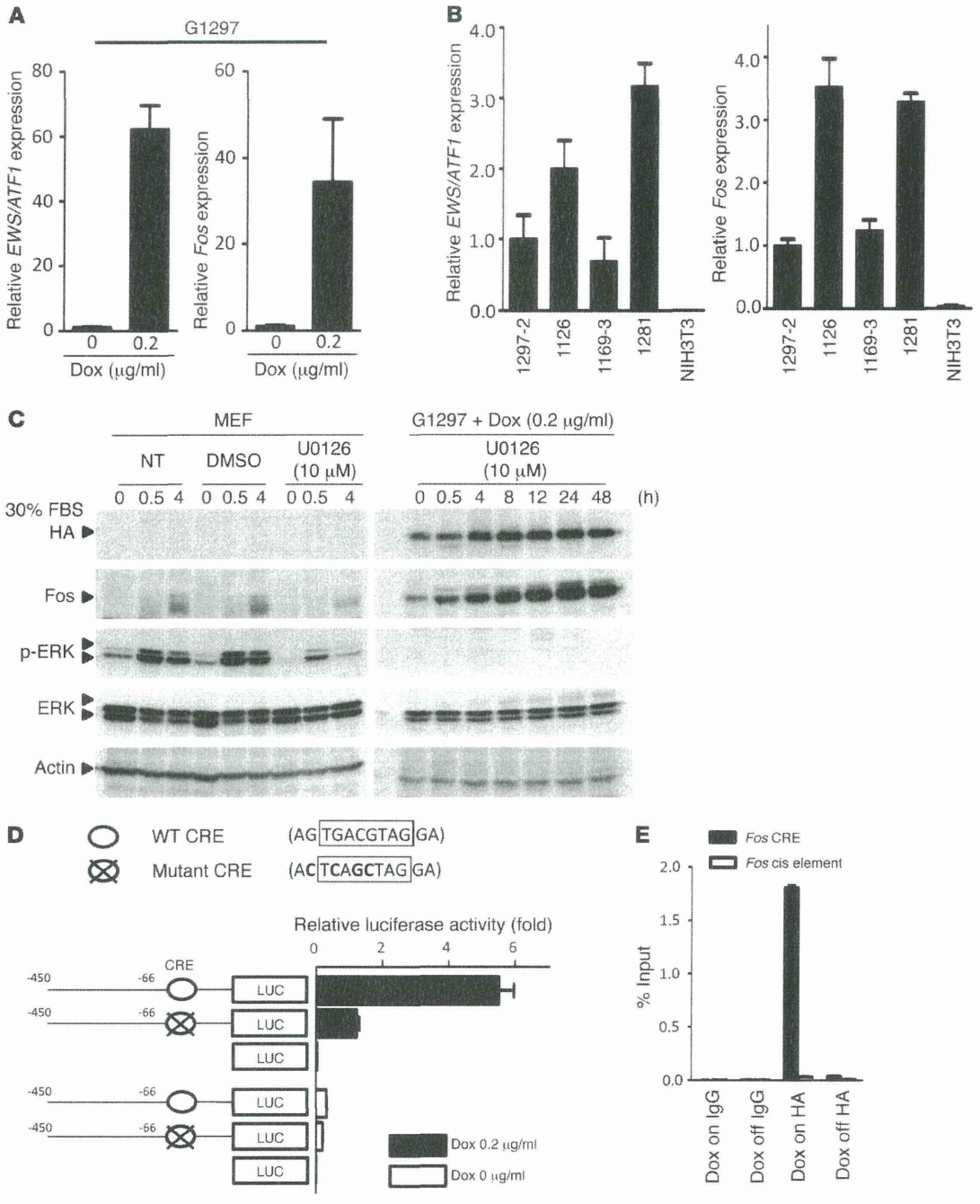

Figure 5

Fos is a direct target of EWS/ATF1. (**A**) Real-time RT-PCR analysis of G1297 cells revealed significant upregulation of both *EWS/ATF1* and *Fos* 3 hours after doxycycline exposure. (**B**) Relative expression of *EWS/ATF1* and *Fos* in 4 *EWS/ATF1*-induced tumors from 4 independent mice. NIH3T3 cells served as a control. Transcript levels were normalized to β-*actin*. Data are mean ± SD (n = 3). (**C**) Fos induction by *EWS/ATF1* was independent of the ERK pathway. Serum-starved MEFs and G1297 cells were stimulated with 30% FBS for the indicated times. Cells were also treated with 10 μM of the MEK inhibitor U0126. Whereas ERK1/2 inhibition by U0126 decreased Fos in MEFs, U0126 failed to suppress Fos expression in G1297 cells. NT, not treated. (**D**) Mouse *Fos* promoter–luciferase reporter constructs and pRL-SV40 vector (as an internal control) were cotransfected in G1297 cells treated with or without 0.2 μg/ml doxycycline. Luciferase activity of each construct was normalized to internal control activity. Data are mean ± SD (n = 3). (**E**) ChIP-PCR analysis was performed for the *Fos* promoter region containing CRE or the negative control cis element using HA-tag antibody or IgG as nonimmune immunoprecipitation, respectively. EWS/ATF1 was enriched at the CRE element of the *Fos* promoter in G1297 cells after treatment with 0.2 μg/ml doxycycline. Data (mean ± SD) were quantified by qRT-PCR and expressed as percent of input DNA.

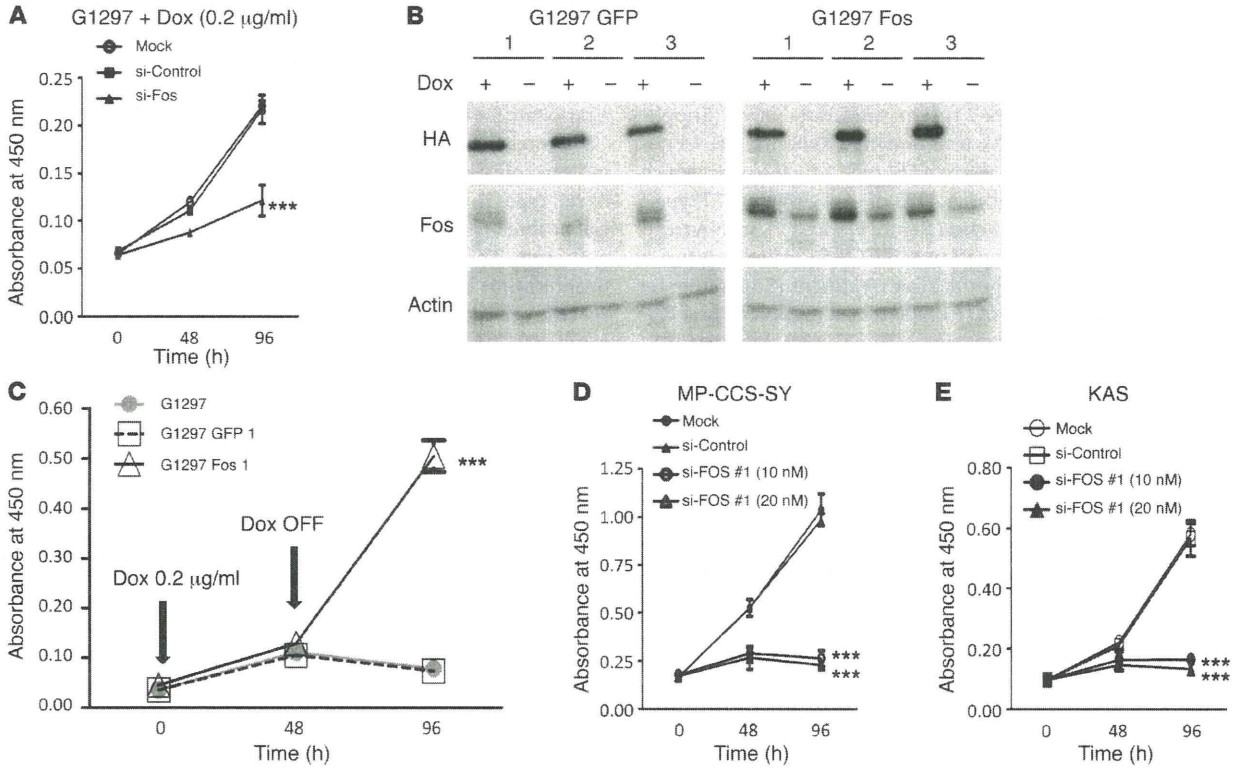

Figure 6

Fos plays a key role in *EWS/ATF1*-induced cell proliferation. (**A**) Effect of *Fos* knockdown on proliferation of *EWS/ATF1*-induced cells. G1297 cells were treated with siRNA targeting *Fos* (si-Fos; 10 nM), a control siRNA (si-Control; 10 nM), or lipofectamine alone (Mock). 48 and 96 hours later, cell viability was determined by WST-8 assay. Results are mean ± SD (n = 4). ***P < 0.001 vs. si-Control and Mock. (**B**) *EWS/ATF1*-induced tumor cell lines overexpressing *Fos* or *EGFP* (G1297 Fos and G1297 GFP, respectively). pCAG-Fos-IZ vector or pCAG-EGFP-IZ vector were stably transfected in G1297 cells. Western blot analysis revealed that G1297 Fos cells stably expressed Fos protein even in the absence of doxycycline. (**C**) Cell proliferation assay for G1297, G1297 GFP, and G1297 Fos cells before and after doxycycline withdrawal. Doxycycline treatment (0.2 μg/ml) was withdrawn for 48 hours. Cell viability was determined by WST-8 assay. ***P < 0.001 vs. G1297 and G1297 GFP. (**D** and **E**) Effect of *FOS* knockdown on growth of human CCS cell lines. MP-CCS-SY and KAS cells were treated with siRNA#1 targeting *FOS* (si-FOS #1; 10 nM and 20 nM), control siRNA (si-Control; 20 nM), or lipofectamine alone (Mock). 48 and 96 hours later, cell viability was determined by WST-8 assay. Data are mean ± SD (n = 4). ***P < 0.001 vs. si-Control and Mock.

(Supplemental Figure 7D), phosphorylation of ERK1/2 was not observed in the *EWS/ATF1*-induced tumor cell line, even after serum stimulation (Supplemental Figure 7E), which suggests that continuous upregulation of Fos in *EWS/ATF1*-induced tumor cells is independent of the RAS/Raf/ERK signaling pathway. We treated *EWS/ATF1*-induced tumor cells with the MEK inhibitor U0126 to block activation of ERK1/2 in order to further confirm the ERK-independent activation of Fos. Although inhibition of ERK1/2 resulted in a substantial decrease of Fos in MEFs, U0126 failed to suppress Fos expression in *EWS/ATF1*-induced tumor cells (Figure 5C). These data indicate that constitutive overexpression of Fos in *EWS/ATF1*-induced tumor cells was mediated by an ERK-independent mechanism.

Previous studies demonstrated an interaction of ATF1 at a CRE in the *Fos* promoter (34, 35), which suggests that EWS/ATF1 may induce *Fos* expression through interaction with the CRE. Conversely, in the present study, regulatory motif analysis of the upregulated genes by EWS/ATF1 demonstrated enrichment of CRE near the transcription start site (from -1,000 bp to +200 bp; Supplemental Figure 6B). To evaluate the functional importance of this element in EWS/ATF1-mediated activation of *Fos*, we constructed a reporter plasmid containing the mouse *Fos* promoter with wild-type and mutated CRE and examined transcriptional activity by luciferase assay (Figure 5D). We confirmed that induction of EWS/ATF1 resulted in remarkably increased *Fos* promoter activity with wild-type CRE in G1297 cells. Importantly, luciferase activity of the mutated promoter significantly decreased compared with that of the wild-type promoter. We further examined whether EWS/ATF1 directly binds to the CRE of the *Fos* promoter. ChIP-PCR analysis revealed that doxycycline-induced EWS/ATF1 was enriched at the CRE of the *Fos* promoter, but not at the negative control cis element (Figure 5E). Our results indicated that the CRE is crucial for EWS/ATF1-mediated transcriptional activity of *Fos* in *EWS/ATF1*-induced tumor cells.

Expression of FOS in human CCS. To investigate whether overexpression of *FOS* is linked to human CCS, we analyzed *FOS* expression in the human CCS cell lines MP-CCS-SY and KAS and in the control lung fibroblast cell line WI38 by qRT-PCR. *FOS* was found to be highly expressed in both human CCS cell lines compared with WI38 (Supplemental Figure 8A). We also found that surgically resected clinical CCS specimens also expressed higher levels of *FOS* than did WI38 (Supplemental Figure 8B), which indicates that human CCS expresses higher levels of *FOS*.